Tip-enhanced Raman Spectroscopy of Graphene

Cassiano Rabelo
Graduate Program in Electrical Eng.
Universidade Federal de Minas Gerais
Belo Horizonte, Brazil
cassianorabelo@ufmg.br

Hudson Miranda
Graduate Program in Electrical Eng.
Universidade Federal de Minas Gerais
Belo Horizonte, Brazil
hudson@labns.com.br

Thiago L. Vasconcelos
Divisão de Metrologia de Materiais
Inmetro
Duque de Caxias, Brazil
tlvasconcelos@inmetro.gov.br

Luiz Gustavo Cançado
Departamento de Física
Universidade Federal de Minas Gerais
Belo Horizonte, Brazil
cancado@fisica.ufmg.br

Ado Jorio
Departamento de Física
Universidade Federal de Minas Gerais
Belo Horizonte, Brazil
adojorio@fisica.ufmg.br

Abstract—This paper presents an optical spectroscopy system engineered to overcome the diffraction limit, describing its building blocks and its application in the characterization of graphene. Based on a technique know as Tip-enhanced Raman Spectroscopy (TERS), the system is capable of obtaining images and spectral information from nanostructures smaller then the minimal length imposed by the diffraction limit of light through the use of optical nanoantennas designed to convert local evanescent radiation to propagating radiation and vice-versa. The system is described with focus on the optical components, including tip-light focus alignment, and on software to handle the massive amount of data generated in hyperspectral imaging. The system is utilized to extract rich information from a graphene nanoflake, with comments on important aspects to generate such spectral analysis.

Index Terms—Optical spectroscopy, Raman spectroscopy, Near-field optical microscopy, Tip-enhanced Raman spectroscopy, Scanning Probe Microscopy

I. INTRODUCTION

Since the XVI century, optical spectroscopy [1] has been used as an important characterization technique capable of providing chemical and structural information from material systems in a non-destructive manner and with little to no impact on the samples' intrinsic properties. As such, it is considered vital for industrial applications and diagnostics, with relevant work being done in biotechnology [2], biofuel [3], soil sciences [4, 5], metrology [6] among other fields far beyond basic science.

Raman spectroscopy is an optical spectroscopy technique based on the inelastic scattering of light [7]. It is capable of providing information about molecular vibrations of a material, allowing not only its chemical and structural identification, but also the quantification of several of its properties. As such, it has been especially important in the study, identification and quantification of defects in nanomaterials such as carbon nanotubes, nanographites and graphenes [8–
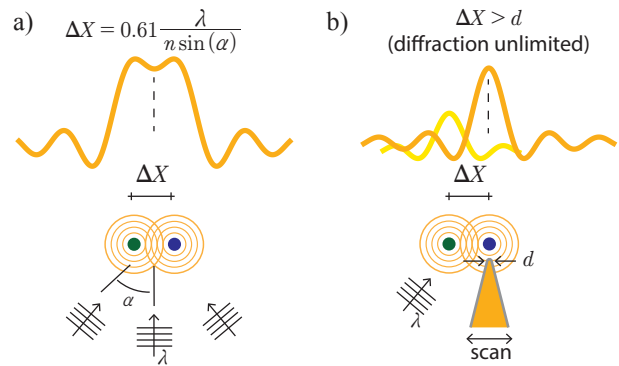
Figure 1. Schematic representation of the Abbe diffraction limit where λ represents the light's wavelength and α represents the half-angle of the focal cone of light. (a) When two objects are closer than ΔX it becomes impossible to resolve them individually. (b) By using a tip with an apex diameter d and being $\Delta X > d$, it is possible to resolve the objects spatially by moving the sample or the tip position (adapted from [12]).

10], considered important prototype materials in the fields of nanoscience and nanotechnology.

However, due to diffraction, propagating light cannot be localized in a region smaller than approximately half of its wavelength, what is known as the Abbe diffraction limit [11] described by the following equation:

$$\Delta X = 0.61 \frac{\lambda}{n \sin(\alpha)} \tag{1}$$

where ΔX is approximately the minimum distance between two distinguishable features of a sample as a function of the light's wavelength λ, the refractive index of the medium n and the half-angle of the focal cone of light α (Fig. 1(a)).

Considering that visible light has a wavelength of $\approx 500\,\mathrm{nm}$, ordinary optical systems are not able to distinguish information in the nanometer scale, limiting its usefulness in nanoscience. The idea on how to overcome this limitation first appeared in 1928 in the work of E. H. Synge [13]. Synge proposed that a sample should be illuminated from

light coming from a source smaller than $\lambda/2$ and, therefore, surpassing the diffraction limit, a technique that would later be named Near-field Scanning Optical Microscopy (NSOM). Although the first NSOM system was only demonstrated in the 1980s [14], these systems evolved at a fast pace and in 2001 reached a milestone in the so-called TERS (Tip-enhanced Raman Spectroscopy) [15].

TERS is a NSOM technique based on the concept of using a metallic tip as a nanoantenna capable of detecting the evanescent or non-propagating waves originated from the interaction of light with sample features smaller than its wavelength, therefore capable of providing structural and chemical information from a sample in a nanometric scale.

Although there exists non-optical techniques capable of providing information from matter in the nanometric scale, such as those in the scanning probe microscopy family, they are not able of providing the chemical information required to reveal the molecular composition of a sample. Also, most of the non-optical methods capable of reaching nanometric scale usually require special sample preparation, precise control of ambient conditions and equipments generally only accessible to research groups with considerable budget.

There is an assortment of systems from various vendors dedicated exclusively to either optical microscopy or SPM and these equipments have been extensively used for years. Their industrial applications range from the study of corrosive agents, lubricants, geology and even tribology studies conducted by the cosmetics industry [16]. The same cannot be said about integrated systems dedicated to TERS measurements. TERS enables the acquisition of a sample's Raman signature with high spatial resolution ($\approx 10\,\mathrm{nm}$) and molecular sensitivity [15] through the combination of a confocal micro-Raman spectroscopy system and an SPM. TERS has already been used to characterize isolated dopant atoms in nanostructures [17] and recently resolutions of $\approx 1\,\mathrm{nm}$ have been achieved [18, 19].

In this paper we present a TERS system, based on a system initially developed Dr. Lukas Novotny (ETH Zurich) and Dr. Achim Hartschuh (LMU Munich) [20], capable of obtaining chemical and structural information, simultaneously, from a sample in the nanometric scale, while performing those measurements in ambient conditions. In section II a description of the TERS system developed is provided, followed by section III where important software developments done in-house to facilitate data analysis and image generation are presented. In Section IV we present the results of successfully analyzing a graphene nanoflake using TERS and being able to acquire optical information beyond the diffraction limit. Finally, in section V, we briefly discuss some plausible implications of using nano-Raman in the analysis of nanostructures.

II. System description

The optical components of a TERS system can be assembled in a myriad of ways. In a possible geometry for the laser/nanoantenna coupling, the laser is incident on the sample through an inverted microscope. On top of this microscope an
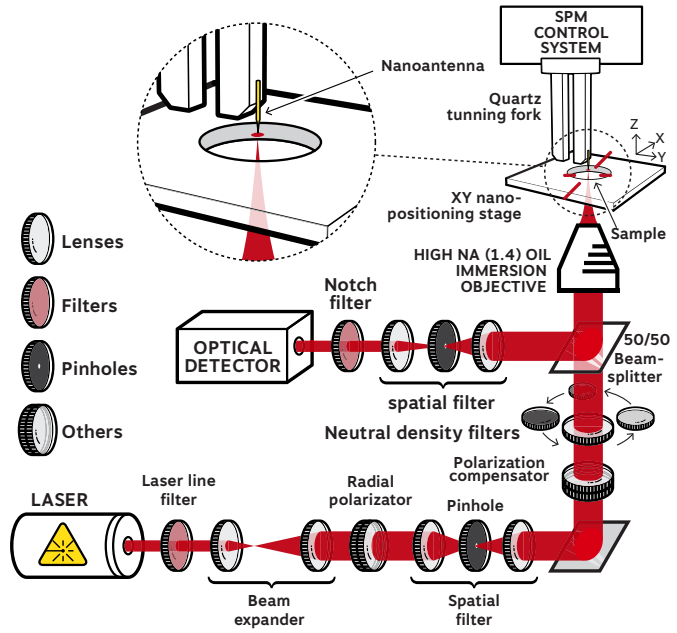

Figure 2. Schematic illustration of the described TERS system with focus on the optical components.

SPM head (or scanhead) is attached (Fig. 2). Unlike most AFM and STM systems commercially available, in the described TERS system, the scanning is done by moving the sample, not the tip, due to the requirement that the laser and nanoantenna must be aligned during the experiment. The sample is fixed to a high-precision nanopositioning scanning stage (X/Y plane) and by moving it, it is possible to obtain spectroscopic and topographic information from any point of the sample within the movement range of the stage. In the described system, the scanning stage is MadCityLabs Nano H-50 with a movement range of $50\,\mu\mathrm{m}$ in X/Y.

The system configuration allows the acquisition of spectroscopic images with nanoscale resolution. It is also possible to carry out spectroscopy measurements (confocal and near-field) in addition to SPM and nanomanipulation measurements using the same probe.

After the interaction with the sample, the collected light can be directed to an APD (Avalanche Photodiode), which is used only for image generation, or to a spectrometer, which can be used for spectral acquisition and hyperspectral imaging (see section III-A).

The APD used is the SPCM-AQRH-14 manufactured by PerkinElmer. Images generated by scanning the sample and acquiring the optical signal with an APD are usually very fast to obtain, being a reliable way to assess the quality of the sample and area under study. One major limitation of an APD lays on its inability to differentiate wavelengths, therefore it only allows us to analyze a given material from the perspective of a single Raman band, and only if the appropriate bandpass filter is available. If the detection of another wavelength is required, it will be necessary to change the bandpass filter and repeat the experiment.

A central component of this system is the R9 controller from RHK Technology. Its function is to control or coordinate the communication of all electronic devices in the system. Among its many functionalities, we can highlight: myriad of voltage sources needed to move the scanning stage, integrate the pulses (TTL) sent by the APD, move the piezoelectric elements contained in the scanhead for positioning the tip, manage the phase-locked loop (PLL) system of the AFM mode, manage bias and current control when operating in STM mode, in addition to limited image processing capabilities.

It is important to note that although the spectrometer has a separate software used for spectra acquisition, the controller must be able to trigger it in order to synchronize the movement of the scanning stage with the spectra obtained by the spectrometer, where for every step of the scanning stage one Raman spectrum is acquired by the spectrometer. Known as hyperspectral image [21] (see section III-A), the final file will contain a complete Raman spectrum for each scanned point. The stored spectrum can later be analyzed and used to generate a single pixel in a final image. For example, to generate an image from a 64 x 64 pixels scan with our system, a total of 4,096 spectra will be stored. Due to the large amount of spectral data acquired during each experiment, helper softwares were developed to parse and analyze the stored data.

One last component is the SPM scanhead. The scanhead has been designed and built in-house and is not commercially available. It works as an ordinary AFM/STM system, with a central piezoelectric element capable of moving the nanoantenna in XY and Z directions.

After finding a suitable region on the sample and having mapped it with a confocal Raman image with an APD, the next step for a TERS experiment is to place the scanhead, with the nanoantenna already mounted, on top of the inverted microscope and to align the tip to the laser focus on the sample.

For the TERS effect to occur, two important aspects must not be neglected: the laser polarization and the perfect lateral alignment of the nanoantenna with the laser focal region.

It is known that when strongly focused, a radially polarized laser beam not only has a smaller spot size than a linearly polarized beam, but more importantly, it presents an electric field longitudinal to its traveling direction at the focus and centered at the optical axis [22]. Due to the geometry of the TERS system (Fig. 2), where the nanoantenna is placed parallel to the beam's direction of propagation, this longitudinal field is fundamental to promote the necessary plasmon oscillations [23] which are, in turn, responsible for a strong local field enhancement at the apex of the nanoantenna and its propagation [24]. The conversion from linear to radial polarization is done by an active element manufactured by the company Arcoptix®.

Regarding the alignment, it is critical that the nanoantenna be perfectly centered with the laser focus area. The first step in the alignment process is a manual one, where, with the help of a long distance microscope with an attached CDD camera, the
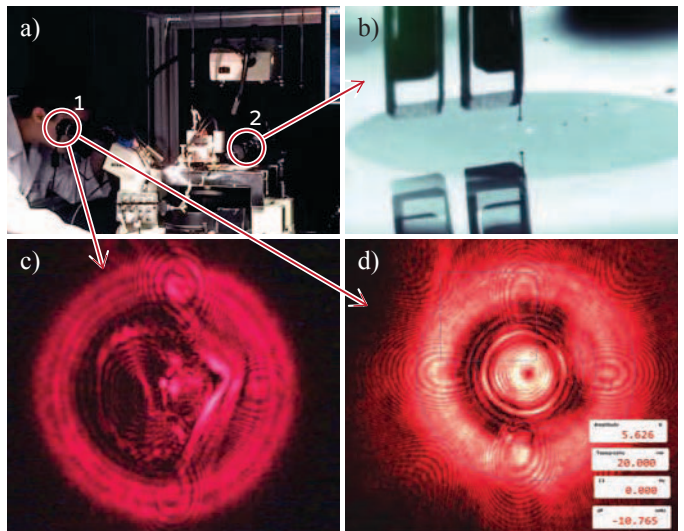

Figure 3. (a) Overview of the system with the eyepiece camera (highlight 1) and the long distance microscope used in the initial alignment process (highlight 2). (b) Image obtained through the camera attached to the long distance microscope. Image obtained through the camera coupled to the eyepiece of the microscope showing the nanoantenna positioned outside the laser focus (c) and correctly positioned in the focal point (d).

tip is lowered towards the sample until it reaches a tip/sample distance $\approx 30\,\mu m$ (Fig. 3(b)).

Once this preliminary alignment is done, an automated tip approach procedure is conducted by the system controller and an additional and more refined alignment of the nanoantenna is necessary, this time using the image generated by a CCD camera attached to the eyepiece of the microscope (Fig. 3(c, d)). This alignment is quite critical and refined, being executed by piezoelectric elements to which the nanoantenna is attached.

III. SOFTWARE DEVELOPMENTS

A. Software for Hyperspectral Image Processing

A hyperspectral surface image comprises a three-dimensional set of data and can be seen as a data parallelogram (Fig. 4), where one of the faces represents the (i, j) spatial coordinates of the final image in the same way as in a two-dimensional image, but stored in each coordinate is a list of numbers representing an entire spectrum. Therefore, a hyperspectral image is composed from dozens, or even thousands of individual spectra, each one contained in a specific row/column - (i, j) - coordinate.

To generate an actual image, one must choose a way to extract a single value from each spectrum contained in each coordinate. The software developed is capable of loading and parsing spectral data acquired and provides a graphical user interface through which the user is able to visualize every single spectra in the dataset. From the selection of one or more bands (Fig. 4(b)), images are generated based the information contained in the selected band. Fig. 4(c, d) show two images obtained by averaging the three largest values inside the selected bands.
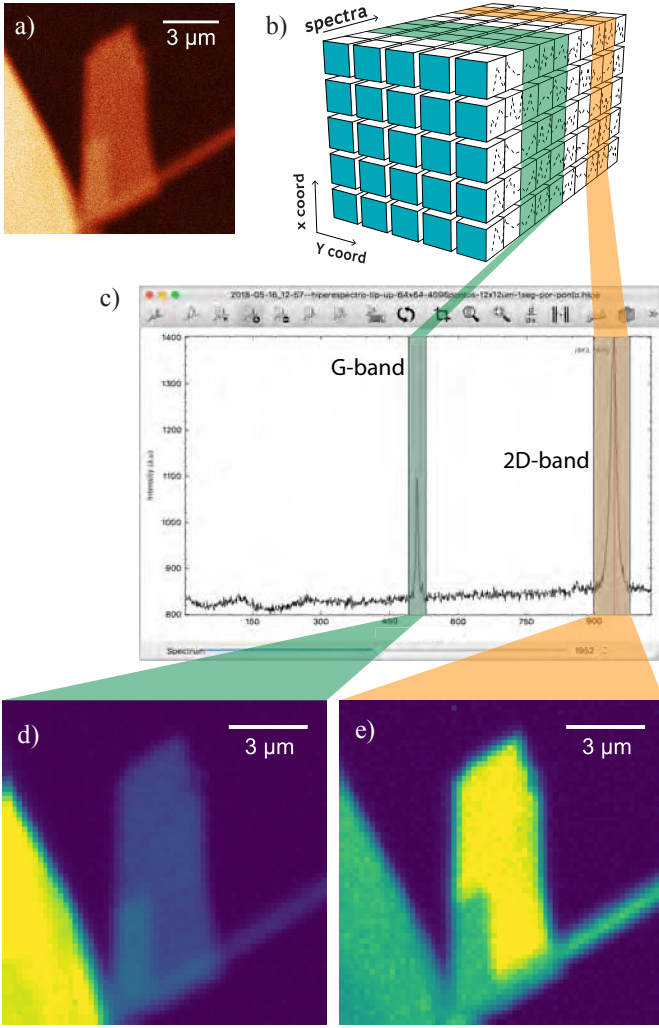
Figure 4. (a) A mechanically exfoliated graphene sample imaged by an APD with a bandpass filter centered on the frequency of the G-band. (b) Representation of a data parallelogram. Each cell in the front face (cyan) corresponds to a measurement location and consequently a pixel in the final image. The axis named "spectra" is the data storage for the spectra acquired, one for each point. The highlighted green and orange areas in the spectra axis corresponds to a band that has been selected to generate the image in (d) and (e). (c) Graphical user interface of hyperspectral image software showing two selected Raman bands used to create (d) and (e). (d) is an image generated from the intensity of the graphene's G-band and (e) is from the intensity of the 2D-band. Both images were synthesized from the same spatial position acquired in a single hyperspectral acquisition.

In spite of the advantages, it is important to emphasize that one of the limitations of the technique is the usually long period of acquisition necessary to obtain the data, where, depending on the signal strength, could take hours to complete. This is due to the low quantum efficiency of spectrometers in general when compared to APDs, therefore, depending on the situation, the use of the technique might be unfeasible.

B. Software for automatic baseline removal and peak fitting of graphene's Raman spectra

A software capable of automatic baseline removal and peak fitting was developed. The software, so far, is specific for
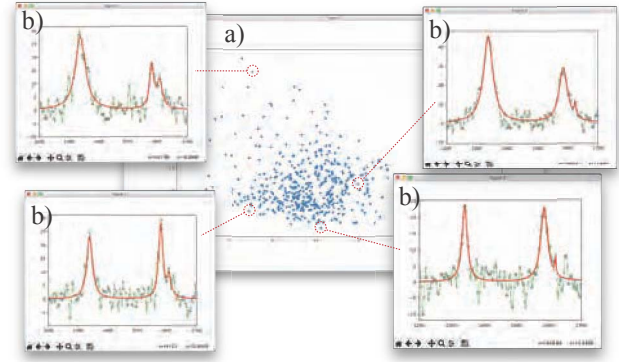

Figure 5. Every single point in (a) originated from the values taken from a successful fit of a single spectrum (see text for details). In (b) we have the original spectrum (green) and the result of the automatic fitting (red) for the selected points.

graphene based materials and limited to fit the D, G, D' and 2D Raman bands of monolayer and multilayer graphene [8].

The software starts with four Lorentzian functions, one for each band, centered according to theory [8, 25]. After an initial fitting round, a series of validation routines are carried out and any band whose fitting parameters do not converge in a desired way or have parameters that are incompatible with that foreseen by the theory, gets automatically marked for exclusion. The developed software uses a number of routines from Peak-o-Mat [26], an open source software for peak fitting.

Fig. 5 shows the result of running the software on a hyperspectral image dataset. A successful fit of the bands exposes all parameters of the fitted Lorentzians for every Raman band. Parameters such as the full width at half maximum (FWHM), the peak intensity, area and position can be obtained for thousands of spectra in one batch. With this information available, meaningful graphs, such the relation between the G-band and 2D-band frequencies, which indicate the amount of strain and doping [27], can be plotted. In Fig. 5(a) we have plotted the FWHM of the G-band versus the area of the D-band over the area of the G-band. Such a graph allows the separation of point and line defects of graphene-related materials [10]. In Fig. 5(b) we show the quality of the fit result for the highlighted points.

IV. TERS OF A GRAPHENE NANOFLAKE

A careful sample preparation is fundamental when planning a TERS experiment. Knowing that the near-field information is only able to propagate a few nanometers before evanescence, a clean sample, with a very clean top surface is required. This is due to the fact that the nanoantenna approaches the sample from above (Fig. 2), therefore, if there are impurities laying over the sample which are thicker than a few nanometers, the near-field would decay even before crossing the tip-sample distance.

Before performing a TERS scan, an APD confocal image of the whole area was acquired, followed by another APD

scan centered on the chosen graphene nanoflake (Fig. 6(a, b)). This graphene nanoflake was extracted from an aqueous graphene solution obtained by the liquid-phase exfoliation method. Notice the inability to spatially resolve the nanoflake due to the diffraction limit.

After that, the tip was engaged and a new scan was made. This time, instead of using an APD to acquire the optical signal, the spectrometer was used in order to generate a hyperspectral image. As already said, this allows the generation of an arbitrary number of images, for each desired Raman band, in a post-scan process. The results of the TERS experiment are shown in Fig. 6.

When comparing the obtained AFM image (Fig. 6(e)) with the images generated from the hyperspectral data (Fig. 6(c, d)) it becomes clear that the nanoflake was optically resolved below the diffraction limit. Fig. 6(f) shows a more than tenfold increase in signal intensity of a spectrum taken with the presence of the nanoantenna (red) when compared with one taken without it (blue) at the location highlighted in Fig. 6(d). This strong signal enhancement is a consequence of the efficient near-field information collection by the nanoantenna used [28]. Also, as shown in Fig. 6(g), due to its ability to capture the local field enclosed by the nanoantenna apex diameter, TERS spectra of distinct regions in the same nanoflake may have different characteristics. Such result would be impossible to achive by micro-Raman.

V. Concluding Remarks

Designing and configuring a tip-enhanced Raman spectroscopy system capable of performing the presented characterizations is not a trivial task. There are several variables involved and all of them are critical to obtain significant improvements in the Raman signal and spatial resolution.

Here we describe a TERS system that is further utilized to generate hyperspectral information from a graphene nanoflake, showing localized defect-induced Raman emissions with spatial resolution down to $10\,\mathrm{nm}$. This paper should be useful for the implementation of similar TERS systems, enabling optical studies and characterization of nanomaterials with resolution below the diffraction limit.
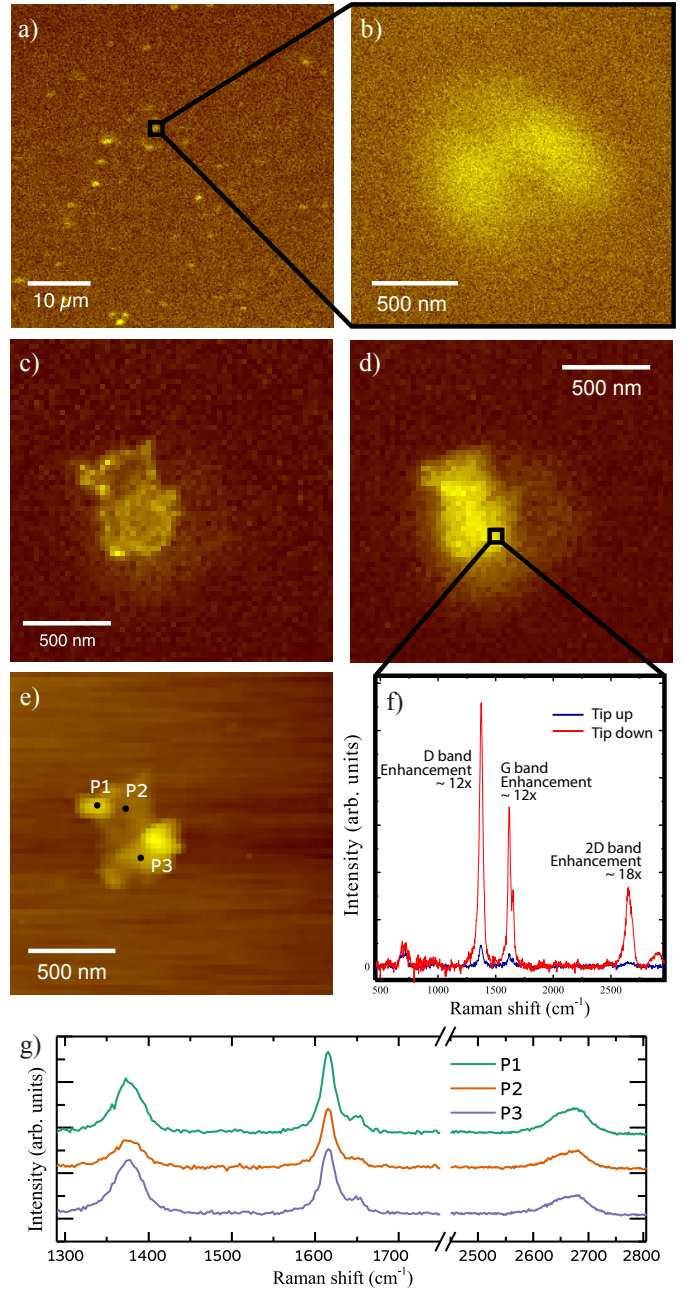
VI. Acknowledgment

Figure 6. TERS results obtained from a sample of graphene nanoflakes. (a) and (b) show confocal micro-Raman images acquired with an APD using a bandpass filter centered on the 2D band and in (b) the scan of an isolated nanoflake within the highlighted area in (a). (c) and (d) are hyperspectral images of the D and G bands, respectively, with a spatial resolution of approximately $10\,\mathrm{nm}$. The images were generated from a hyperspectrum obtained with TERS. (e) shows an AFM topography image obtained during the hyperspectral image scan. In (f) we have the Raman spectrum obtained at the point marked in (d) with the presence of the tip (tip down - red) and without the tip (tip up - blue). (g) Spectra P1, P2 and P3 where taken from points in (e).

References

[1] M. Baudelet, *Laser Spectroscopy for Sensing: Fundamentals, Techniques and Applications*. Elsevier, 2014.

[2] M. Ladeira, V. Andrade, E. Gomes, C. Aguiar, E. Moraes,

J. Soares, E. Silva, R. Lacerda, L. Ladeira, A. Jorio *et al.*, "Highly efficient sirna delivery system into human and murine cells using single-wall carbon nanotubes," *Nanotechnology*, vol. 21, no. 38, p. 385101, 2010.

[3] M. M. Maru, M. M. Lucchese, C. Legnani, W. G. Quirino, A. Balbo, I. B. Aranha, L. T. Costa, C. Vilani, L. Á. de Sena, J. C. Damasceno *et al.*, "Biodiesel compatibility with carbon steel and hdpe parts," *Fuel Processing Technology*, vol. 90, no. 9, pp. 1175–1182, 2009.

[4] A. Jorio, J. Ribeiro-Soares, L. Cançado, N. Falcao, H. Dos Santos, D. Baptista, E. M. Ferreira, B. Archanjo, and C. Achete, "Microscopy and spectroscopy analysis of carbon nanostructures in highly fertile amazonian anthrosoils," *Soil and Tillage Research*, vol. 122, pp. 61–66, 2012.

[5] J. Ribeiro-Soares, L. Cancado, N. Falcao, E. Martins Ferreira, C. Achete, and A. Jorio, "The use of raman spectroscopy to characterize the carbon materials found in amazonian anthrosoils," *Journal of Raman Spectroscopy*, vol. 44, no. 2, pp. 283–289, 2013.

[6] B. Archanjo, I. Maciel, E. M. Ferreira, S. Peripolli, J. Damasceno, C. Achete, and A. Jorio, "Ion beam nanopatterning and micro-raman spectroscopy analysis on hopg for testing fib performances," *Ultramicroscopy*, vol. 111, no. 8, pp. 1338–1342, 2011.

[7] N. Colthup, *Introduction to infrared and Raman spectroscopy*. Elsevier, 2012.

[8] A. Jorio, M. S. Dresselhaus, R. Saito, and G. Dresselhaus, *Raman spectroscopy in graphene related systems*. John Wiley & Sons, 2011.

[9] A. Jorio, G. Dresselhaus, and M. S. Dresselhaus, *Carbon nanotubes: advanced topics in the synthesis, structure, properties and applications*. Springer Science & Business Media, 2007, vol. 111.

[10] L. G. Cançado, M. G. Da Silva, E. H. M. Ferreira, F. Hof, K. Kampioti, K. Huang, A. Pénicaud, C. A. Achete, R. B. Capaz, and A. Jorio, "Disentangling contributions of point and line defects in the raman spectra of graphene-related materials," *2D Materials*, vol. 4, no. 2, p. 025039, 2017.

[11] E. Abbe, "On the estimation of aperture in the microscope." *Journal of the Royal Microscopical Society*, vol. 1, no. 3, pp. 388–423, 1881.

[12] L. Novotny and S. J. Stranick, "Near-field optical microscopy and spectroscopy with pointed probes," *Annu. Rev. Phys. Chem.*, vol. 57, pp. 303–331, 2006.

[13] E. Synge, "Xxxviii. a suggested method for extending microscopic resolution into the ultra-microscopic region," *The London, Edinburgh and Dublin Philosophical Mag. and Journal of Science*, vol. 6, no. 35, pp. 356–362, 1928.

[14] A. Lewis, M. Isaacson, A. Harootunian, and A. Muray, "Development of a 500 å spatial resolution light microscope: I. light is efficiently transmitted through $\lambda/16$ diameter apertures," *Ultramicroscopy*, vol. 13, no. 3, pp. 227–231, 1984.

[15] R. M. Stöckle, Y. D. Suh, V. Deckert, and R. Zenobi, "Nanoscale chemical analysis by tip-enhanced raman spectroscopy," *Chemical Physics Letters*, vol. 318, no. 1, pp. 131–136, 2000.

[16] D. G. Yablon, *Scanning probe microscopy for industrial applications: nanomechanical characterization*. John Wiley & Sons, 2013.

[17] I. O. Maciel, N. Anderson, M. A. Pimenta, A. Hartschuh, H. Qian, M. Terrones, H. Terrones, J. Campos-Delgado, A. M. Rao, L. Novotny *et al.*, "Electron and phonon renormalization near charged defects in carbon nanotubes," *Nature materials*, vol. 7, no. 11, p. 878, 2008.

[18] R. Zhang, Y. Zhang, Z. Dong, S. Jiang, C. Zhang, L. Chen, L. Zhang, Y. Liao, J. Aizpurua, Y. Luo *et al.*, "Chemical mapping of a single molecule by plasmon-enhanced raman scattering," *Nature*, vol. 498, no. 7452, pp. 82–86, 2013.

[19] J. Lee, K. T. Crampton, N. Tallarida, and V. A. Apkarian, "Visualizing vibrational normal modes of a single molecule with atomically confined light," *Nature*, vol. 568, no. 7750, p. 78, 2019.

[20] A. Hartschuh, E. J. Sánchez, X. S. Xie, and L. Novotny, "High-resolution near-field raman microscopy of single-walled carbon nanotubes," *Physical Review Letters*, vol. 90, no. 9, p. 095503, 2003.

[21] L. Wang and C. Zhao, *Hyperspectral image processing*. Springer, 2016.

[22] R. Dorn, S. Quabis, and G. Leuchs, "Sharper focus for a radially polarized light beam," *Physical Review Letters*, vol. 91, no. 23, p. 233901, 2003.

[23] L. Novotny, R. X. Bian, and X. S. Xie, "Theory of nanometric optical tweezers," *Physical Review Letters*, vol. 79, no. 4, p. 645, 1997.

[24] T. L. Vasconcelos, B. S. Archanjo, B. Fragneaud, B. S. Oliveira, J. Riikonen, C. Li, D. S. Ribeiro, C. Rabelo, W. N. Rodrigues, A. Jorio *et al.*, "Tuning localized surface plasmon resonance in scanning near-field optical microscopy probes," *ACS nano*, vol. 9, no. 6, pp. 6297–6304, 2015.

[25] A. C. Ferrari, J. Meyer, V. Scardaci, C. Casiraghi, M. Lazzeri, F. Mauri, S. Piscanec, D. Jiang, K. Novoselov, S. Roth *et al.*, "Raman spectrum of graphene and graphene layers," *Physical review letters*, vol. 97, no. 18, p. 187401, 2006.

[26] "Peak-o-mat," https://sourceforge.net/projects/lorentz/, 2017, [Online; accessed 2017-12-19].

[27] J. E. Lee, G. Ahn, J. Shim, Y. S. Lee, and S. Ryu, "Optical separation of mechanical strain from charge doping in graphene," *Nature Communications*, vol. 3, p. 1024, 2012.

[28] T. L. Vasconcelos, B. S. Archanjo, B. S. Oliveira, R. Valaski, R. C. Cordeiro, H. G. Medeiros, C. Rabelo, A. Ribeiro, P. Ercius, C. A. Achete *et al.*, "Plasmon-tunable tip pyramids: Monopole nanoantennas for near-field scanning optical microscopy," *Advanced Optical Materials*, vol. 6, no. 20, p. 1800528, 2018.